Biochimica et Biophysica Acta 1837 (2014) 112–120

Contents lists available at ScienceDirect

Biochimica et Biophysica Acta

journal homepage: www.elsevier.com/locate/bbabio

Electrochemically driven catalysis of *Rhizobium* sp. NT-26 arsenite oxidase with its native electron acceptor cytochrome c_{552}

Palraj Kalimuthu [a], Matthew D. Heath [b], Joanne M. Santini [b], Ulrike Kappler [a], Paul V. Bernhardt [a,*]

[a] School of Chemistry and Molecular Biosciences, University of Queensland, Brisbane 4072, Australia
[b] Institute of Structural and Molecular Biology, University College London, WC1E 6BT, UK

ARTICLE INFO

Article history:
Received 9 May 2013
Received in revised form 5 July 2013
Accepted 19 July 2013
Available online 26 July 2013

Keywords:
Molybdenum
Enzyme
Voltammetry
Arsenite
Cytochrome

ABSTRACT

We describe the catalytic voltammograms of the periplasmic arsenite oxidase (Aio) from the chemolithoautotrophic bacterium *Rhizobium* sp. str. NT-26 that oxidizes arsenite to arsenate. Electrochemistry of the enzyme was accomplished using its native electron transfer partner, cytochrome c_{552} (cyt c_{552}), as a mediator. The protein cyt c_{552} adsorbed on a mercaptoundecanoic acid (MUA) modified Au electrode exhibited a stable, reversible one-electron voltammetric response at +275 mV *vs* NHE (pH 6). In the presence of arsenite and Aio the voltammetry of cyt c_{552} is transformed from a transient response to an amplified sigmoidal (steady state) wave consistent with an electro-catalytic system. Digital simulation was performed using a single set of parameters for all catalytic voltammetries obtained at different sweep rates and various substrate concentrations. The obtained kinetic constants from digital simulation provide new insight into the kinetics of the NT-26 Aio catalytic mechanism.

1. Introduction

Although various chemical forms of arsenic can be found in the natural environment, arsenic in water mainly occurs in two forms, trivalent arsenite ($As(OH)_3$) and pentavalent arsenate (present as $HAsO_4^{2-}$ and $H_2AsO_4^-$ at neutral pH) [1,2]. Arsenite is significantly more toxic to humans than arsenate due to its high affinity for sulfhydryl groups of proteins and dithiols such as glutaredoxin which may disrupt intracellular oxidation–reduction homeostasis [3,4]. The chemical oxidation of arsenite to arsenate is very slow and therefore, most arsenite oxidation takes place through microbial action. The Mo-dependent arsenite oxidases (Aio) [5] are the enzymes that carry out this two electron oxidation reaction (As(III) to As(V)) which is important in the cycling of arsenic in the environment. The first arsenite-oxidizing bacterium, *Bacillus arsenoxydans* was isolated by Green [6] from an arsenical cattle dip in 1918 and more recently Aio enzymes have been isolated from a variety of bacteria including *Alcaligenes faecalis*, *Rhizobium* sp. str. NT-26, *Hydrogenophaga* sp. str. NT-14, *Arthrobacter* sp. str. 15b, *Polaromonas* sp. str. GM1 and *Ralstonia* sp. str. 22 [7–12].

The most intensively studied arsenite oxidase is from the heterotrophic bacterium *A. faecalis* which is a member of the Betaproteobacteria [9,13,14]. *A. faecalis* Aio is a periplasmic heterodimeric enzyme comprising three distinct electron transfer cofactors; the Mo active site and an adjacent high potential [3Fe–4S] cluster within the α-AioA unit and a Rieske type (His-coordinated) [2Fe–2S] center in the β-AioB unit [15]. The active site comprises two bidentate molybdopterin ligands and a terminal oxido ligand bound to Mo thus placing it within the DMSO reductase family of Mo enzymes [16,17]. The AioB subunit is similar to the Rieske iron sulfur proteins of the cytochrome bc_1 and b_6f complexes [9]. There are many unusual structural features of Aio enzymes that set them apart from other members of the DMSO reductase family. Most notable is the absence of an amino acid side-chain in the coordination sphere, unlike other members of the DMSO reductase family where Ser, Cys, Se-Cys, and Asp residues have been identified [13]. Indeed there are no covalent or coordinate bonds connecting the Mo cofactor and the peptide chain [18]. In place of the amino acid ligand it has been suggested that a spectator oxido ligand is present on the basis of EXAFS studies on *A. faecalis* Aio [13] and on crystallographic and spectroscopic studies on small molecule Mo complex analogs that bear similar ligands to the Aio active site [19].

The catalytic mechanism of arsenite oxidation at the Mo active site is illustrated in Scheme 1 [18]. Nucleophilic attack by $As(OH)_3$ on the $O = Mo^{VI}$ oxido ligand (through the As lone pair) leads to an arsenato ligand coordinated to Mo^{IV}. Two electron arsenite oxidation coupled with two electron reduction of the Mo ion (Mo^{VI} to Mo^{IV}) is typical behavior for all Mo oxidase/dehydrogenase enzymes [17]. Interestingly the intermediate EPR-active oxidation state (Mo^V) has never been observed in an Aio, which is atypical in Mo enzymology [20]. This is due to the potential of the $Mo^{VI/V}$ couple being either close to, or lower than, the $Mo^{V/IV}$ couple rendering the Mo^V state unstable to disproportionation. In the reductive half-reaction, the catalytic cycle is completed by dissociation of arsenate from Mo^{IV}. The oxidative half reaction involves intramolecular electron transfer from Mo^{IV} to the Rieske center *via* the [3Fe–4S] cluster.

Rhizobium sp. str. NT-26 Aio (NT-26 Aio) was isolated from the Granites gold mine, Northern Territory, Australia [21]. It is a member of

* Corresponding author. Tel.: +61 7 3365 4266; fax: +61 7 3365 4299.
E-mail address: p.bernhardt@uq.edu.au (P.V. Bernhardt).

0005-2728/$ – see front matter © 2013 Elsevier B.V. All rights reserved.
http://dx.doi.org/10.1016/j.bbabio.2013.07.010

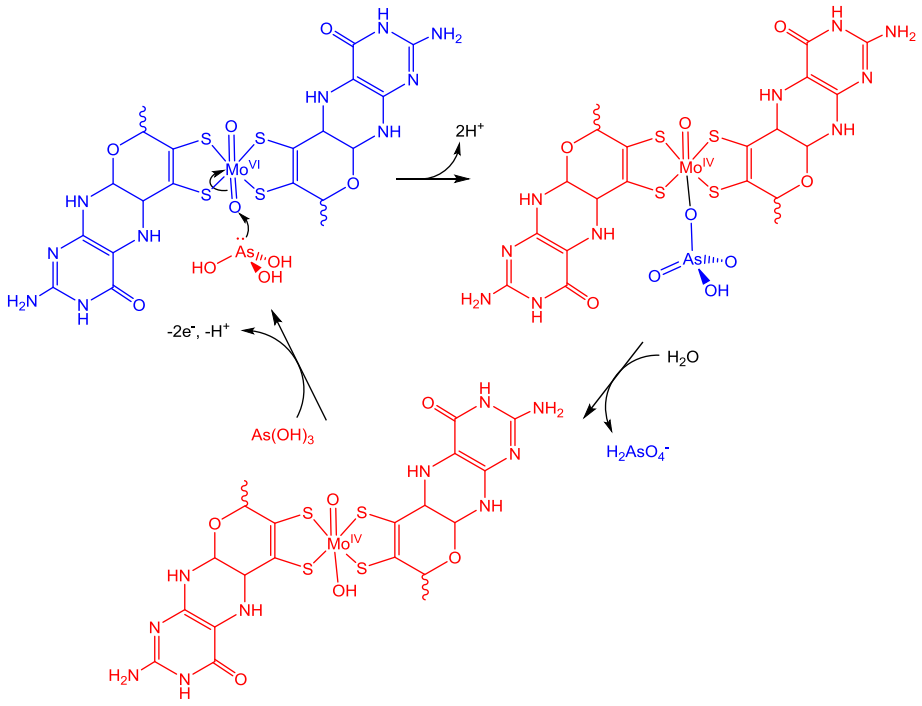

Scheme 1. Reaction mechanism for Aio-catalyzed arsenite oxidation. The spectator ligand is shown as oxido but its identity remains unresolved.

the Alphaproteobacteria and can grow both chemolithoautotrophically and heterotrophically with arsenite as the electron donor [21]. Aio contains two heterologous subunits, AioA and AioB, with molecular masses of 98 kDa and 14 kDa, respectively. Based on the estimated molecular mass of 219 kDa this suggests an $\alpha_2\beta_2$ heterotetrameric structure which was supported by ICP-MS analysis which revealed the presence of 2.02 ± 0.08 atoms of Mo and 9.2 ± 0.6 atoms of Fe per tetramer. These results are consistent with the same cofactor composition identified in the crystallographically characterized *A. faecalis* Aio (an αβ dimer) [18]. EPR analysis of NT-26 Aio also confirmed that the Fe–S clusters of this enzyme are similar to those of the *A. faecalis* Aio [22]. Sequence analysis reveals that NT-26 Aio has a similar domain structure (but not sequence similarity) to other Aio homologues from *Aeropyrum pernix*, *Sulfolobus tokodaii* and *Chloroflexus aurantiacus* [7].

In an earlier report we demonstrated the direct catalytic electrochemistry of NT-26 Aio on an edge plane pyrolytic graphite (EPG) electrode using polymixin sulfate as promoter to enhance the surface coverage of the electroactive enzyme [23]. The obtained kinetic parameters were comparable with conventional solution assays [7] and suggested that NT-26 Aio functions natively while adsorbed on the EPG electrode surface. However, no non-turnover voltammetric responses were found from any of the enzyme cofactors in the absence of arsenite due to the low overall surface coverage of the enzyme [23].

Herein, we report the mediated catalytic voltammetry of NT-26 Aio partnered with its physiological electron acceptor cyt c_{552} on a mercaptoundecanoic acid (MUA)-modified Au electrode. In a previous publication [24] we obtained a voltammetric response from the heme cofactor in cyt c_{552} at a glassy carbon electrode coated with a polystyrene sulfonate polymer (Eastman AQ); the redox potential was +217 mV vs. NHE (pH 7.1). However, the method employed required a high concentration of cyt c_{552} to be in contact with the electrode and this is impractical in an enzyme coupled system where similar concentrations of Aio and cytochrome are required.

It is known that recombinant cyt c_{552} possesses a pI of 6.77 [24] and therefore we took a different approach by employing a negatively charged self-assembled monolayer of carboxylate terminated long chain thiols attached to a Au electrode [25,26] to provide a more organized layer that would attract the protein while still allowing some degree of mobility at the electrode surface so that it may interact with both the electrode and its redox partner NT-26 Aio. The electrocatalytic activity of the NT-26 Aio/cyt c_{552} system is investigated here and these results are compared with our reported direct electrochemistry of NT-26 Aio [23]. Further, we have employed electrochemical simulation to explore the kinetics of this system including the Aio–arsenite reaction and the Aio–cyt c_{552} reaction.

2. Experimental section

2.1. Materials

The enzyme NT-26 Aio was prepared using a heterologous expression system in *E. coli* as described [27]. Aliquots of Aio at concentrations of 26 μM were used for all experiments. The protein cyt c_{552} (64 μM) was prepared as previously described [24]. Purified NT-26 Aio and cyt c_{552} were stored at −70 °C. 11-mercaptoundecanoic acid and sodium meta-arsenite ($NaAsO_2$) were purchased from Aldrich and were used as received. All other chemicals used were of analytical grade purity and used without further purification. Perm-selective dialysis membranes (MW cut off 3500 Da) were obtained from SERVA Electrophoresis, Germany. All solutions were prepared with ultrapure water (resistivity 18.2 MΩ cm) from a Millipore Milli-Q system. Phosphate buffer solution (100 mM) was used for experiments at pH 6.0. The pH dependent experiments were carried out in the range of 4.5 to 7.5 and desired pH was obtained by a mixture of 0.1 M citric acid and 0.2 M Na_2HPO_4 [28].

2.2. Electrochemical measurements and electrode cleaning

Cyclic voltammetry (CV) was carried out with a BAS 100B/W electrochemical workstation coupled with a BAS RDE-3 rotating disk electrode cell stand. A three-electrode system was employed comprising a gold disk working electrode, a Pt wire counter, and a Ag/AgCl reference electrode (+196 mV vs. NHE). Experiments were carried out with 30 min argon purged solutions and also an argon blanket was maintained during the measurement. The Au working electrode was mechanically, chemically, and electrochemically cleaned and polished

according to a published procedure [29]. The monolayer of 11-mercaptoundecanoic acid (MUA) was prepared on a clean Au electrode by immersion in a 10 mM ethanolic solution of MUA for 24 h [30]. The electrode was subsequently washed with copious amounts of ethanol and water to remove any loosely bound MUA molecules from the electrode surface. The voltammetry was carried out at different temperatures in the range 5 to 25 °C using Colora Kryo-Thermostat connected with a water jacketed electrochemical cell.

The electro-active surface area of the Au electrode (A) was determined by CV analysis of a 1 mM ferrocene methanol in a 0.1 M KCl solution at different sweep rates using the Randles–Sevcik equation (Eq. (1)) [31]. The diffusion coefficient (D_o) of ferrocene methanol [32] is 6.7×10^{-6} cm^2 s^{-1}, i_p is the measured current maximum, the number of electrons n = 1, the concentration of analyte is $C_o = 10^{-6}$ mol cm^{-3}, and v is the sweep rate (V s^{-1}).

$$i_p = \left(2.69 \times 10^5\right) n^{3/2} A D_o{}^{1/2} C_o v^{1/2} \quad (1)$$

The pH dependence of the catalytic current was modeled by Eq. (2) which is applicable for an enzyme that is deactivated by either a deprotonation (pK_{a1}) or protonation (pK_{a2}) reaction [33].

$$i_{lim}(pH) = \frac{i_{opt}}{1 + 10^{(pH - pK_{a1})} + 10^{(pK_{a2} - pH)}} \quad (2)$$

2.3. Enzyme electrode preparation

A mixture of 1 μL of NT-26 Aio (26 μM) and 4 μL of cyt c_{552} (64 μM) in MES buffer was pipetted onto the conducting surface of an inverted, freshly prepared Au/MUA working electrode and this was allowed to dry to a film at 4 °C. To prevent protein loss the electrode surface was carefully covered with a perm-selective dialysis membrane (MW cut off 3500 Da), presoaked in water. The dialysis membrane was pressed onto the electrode with a Teflon cap and fastened to the electrode with a rubber O-ring to prevent leakage of the internal membrane solution. The resulting modified electrode was stored at 4 °C in 100 mM phosphate buffer (pH 6.0) when not in use.

2.4. Electrochemical simulation

The experimental cyclic voltammograms (CVs), were simulated with the DigiSim program (version 3.03b) [34]. The working electrode surface area (0.067 cm^2) determined as described above was assumed to be the same for each experiment and the double-layer capacitance was found to be 5 μF from the separation of the baseline anodic and cathodic currents. It is assumed that both NT-26 Aio and cyt c_{552} are adsorbed on Au/MUA electrode surface and arsenite is under diffusion control. Therefore, finite diffusion was assumed and all pre-equilibration reactions were disabled. NT-26 Aio and cyt c_{552} adsorbed to the Au/MUA electrode were treated as confined to a thin layer (unable to diffuse away from this layer, the so-called blocked boundary conditions) while arsenite was free to diffuse and cross the membrane (Scheme 2). The apparent redox potential of cyt c_{552} was determined from control experiments in the absence of NT-26 Aio or arsenite. The diffusion coefficient of cyt c_{552} was also estimated by simulation of its cyclic voltammetry at varying sweep rates in the absence of substrate and enzyme and obtained as 5.0×10^{-6} cm^2 s^{-1} which is consistent with the values reported for other *c*-type cytochromes [35]. The diffusion coefficients for NT-26 Aio and arsenite were taken to be 1×10^{-7} and 1×10^{-5} cm^2 s^{-1}. These values were kept constant for simulating the various substrate concentration dependent CVs. The heterogeneous rate constant was determined from simulating the sweep rate dependence of the anodic peak to cathodic peak separation of mediators (in the absence of NT-26 Aio) and then held constant during the simulations of different sweep rate and substrate concentration dependent catalytic voltammetries. The only values that were allowed to vary were the homogenous rate and equilibrium constants shown in Scheme 2.

3. Results and discussion

3.1. Electrocatalytic mechanism of NT-26 Aio

NT-26 Aio has three active redox cofactors; the Mo center, the [3Fe–4S] cluster and the Rieske [2Fe–2S] cluster [7]. Based on the arrangement of these cofactors identified in the crystal structure of *A. faecalis* Aio [18], electrons generated by the oxidation of arsenite follow the path Mo → [3Fe–4S] → [2Fe–2S] with both Fe–S clusters transferring one electron at a time. From the Rieske [2Fe–2S] cluster, the electrons are then transferred to the periplasmic electron acceptor cyt c_{552} [24].

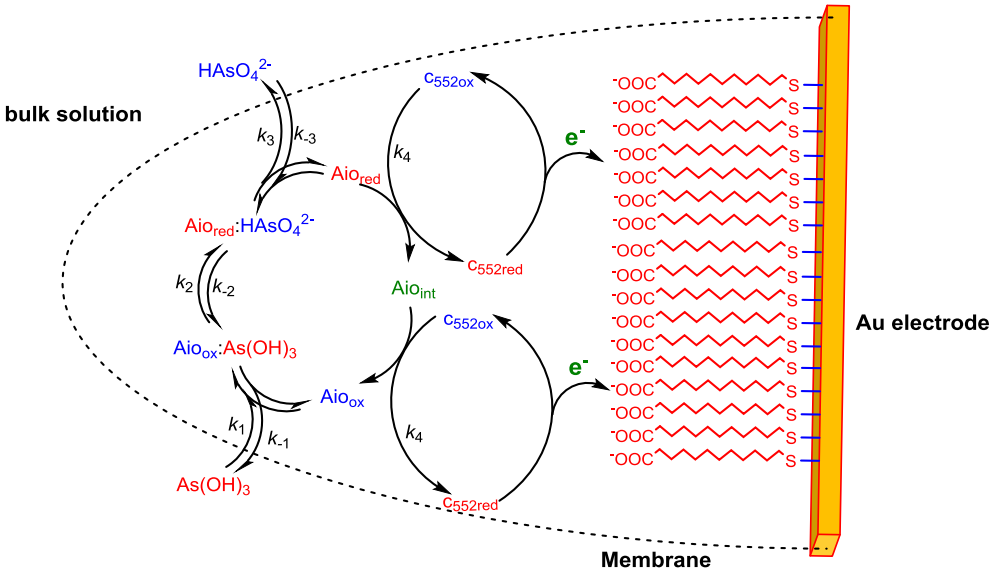

Scheme 2. Mediated electrochemically driven catalysis of NT-26 Aio.

We have assumed that the catalytic reaction follows Michaelis–Menten kinetics and consists of (non-covalent) arsenite binding (k_1/k_{-1}), turnover (k_2/k_{-2}) and arsenate release (k_3/k_{-3}). A simplified double substrate 'ping-pong' mechanism was employed to model the overall reaction kinetics as described in Scheme 2. In the reductive half reaction, arsenite binds to the oxidized active site (k_1) of Aio and nucleophilic attack by the As lone pair on the oxido ligand of Mo^{VI} generating a coordinated arsenato ligand (k_2), then arsenate dissociates from the active site (k_3) [18].

In the oxidative half reaction, the cyt c_{552} mediator oxidizes Aio in two consecutive outer sphere electron transfer reactions (k_4) via an intermediate one electron reduced form Aio_{int}. Internal electron transfer (Mo to [3Fe–4S] then [2Fe–2S]) is assumed to be rapid and not rate-limiting. The redox potential of the Rieske [2Fe–2S] cluster in NT-26 Aio is +225 mV vs. NHE [22]. The potential of the [3Fe–4S] cluster is around +270 mV [20]. Given that no Mo^V EPR signal has been observed from any Aio the $Mo^{VI/V}$ and $Mo^{V/IV}$ redox potentials remain unknown but the absence of a stable Mo^V signal indicates that $E(Mo^{VI/V}) \leq E(Mo^{V/IV})$. On this basis it appears that the electronic configurations of the three redox states of the enzyme are $Aio_{ox} = Mo^{VI}$:$[3Fe–4S]_{ox}$:$[2Fe–2S]_{ox}$; $Aio_{red} = Mo^{IV}$:$[3Fe–4S]_{ox}$:$[2Fe–2S]_{ox} \leftrightarrow Mo^{VI}$:$[3Fe–4S]_{red}$:$[2Fe–2S]_{red}$ and $Aio_{int} = Mo^{VI}$:$[3Fe–4S]_{red}$:$[2Fe–2S]_{ox}$. In other words the two Fe–S clusters act in tandem to effectively remove two electrons from the Mo^{IV} active site synchronously following arsenite oxidation and no Mo^V signal ever accumulates.

3.2. Cytochrome c_{552} voltammetry

Fig. 1 shows the cyclic voltammetry response of cyt c_{552} at the Au/MUA working electrode (pH 6) at different sweep rates. Here 4 μL of a 64 μM solution of cyt c_{552} was trapped beneath the membrane covering the electrode and unable to diffuse into the bulk solution (Scheme 2). A well-defined redox wave centered at +275 mV (vs. NHE) with a peak to peak separation of 35 mV was obtained at 10 mV s^{-1} (pH 6.0). The observed redox wave corresponds to the oxidized and reduced forms of cyt c_{552} i.e. the ferric and ferrous forms of the cytochrome [35–37].

Earlier, we reported the redox potential of cyt c_{552} using (equilibrium) redox potentiometry (+251 mV vs. NHE at pH 6.5) and cyclic voltammetry at a glassy carbon electrode modified with the Eastman AQ29 polyester sulfonate (+218 mV vs. NHE at pH 7.1). The slightly lower redox potentials measured at the glassy carbon/polyester sulfonate electrode compared with the present Au/MUA/cyt c_{552} system (+275 mV vs. NHE at pH 6) may be due to different interactions between the protein and the surface modifiers, particularly their different terminal groups (sulfonate vs. carboxylate).

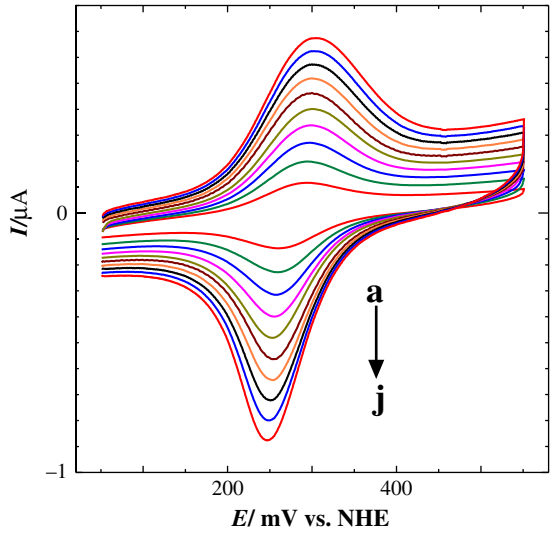

Fig. 1. CVs obtained for 4 μL of cyt c_{552} on Au/MUA electrode at different scan rates (a) 10, (b) 20, (c) 30, (d) 40, (e) 50, (f) 60, (g) 70, (h) 80, (i) 90 and (j) 100 mV s^{-1} in 100 mM phosphate buffer (pH 6).

The voltammetry of cyt c_{552} at the Au/MUA electrode is pH independent within the range 4 < pH < 7 (Supporting information S1). At pH 8 the anodic and cathodic peaks separate but their average potential remains the same. The broadening is most likely linked with a weakening of the electrostatic attraction between cyt c_{552} (pI 6.77) and the negatively charged SAM ($-CO_2^-$ terminated) electrode as fewer positively charged surface amino acid residues remain. The key point is that there is no change in redox potential in this range so the redox reaction is not coupled with any protonation events at the heme.

These results also show that native activity of cyt c_{552} is retained on the Au/MUA electrode. Further, the electrochemical response of cyt c_{552} is very stable on the Au/MUA electrode due to electrostatic attraction of remaining positively charged amino acid side chains with the negatively charged MUA monolayer [25]. The anodic current increased with scan rate but neither linearly (R^2 0.986), as expected for surface adsorbed protein [31], or with the square root of scan rate (R^2 0.968) as would be expected from a purely diffusion controlled electron transfer (see Supporting information Fig. S2). The small peak-to peak separation (35 mV less than the theoretical 57 mV for a single electron diffusion controlled response at 298 K) indicates that some of the response is from a surface confined cytochrome but the absence of a true linear relationship and the concentration dependence of the observed current are a convolution of both diffusional and surface adsorbed voltammetry. For the diffusional component of the current, Eq. (1) allows an estimate of an upper bound of the protein concentration (~120 μM) using the electroactive surface area (A = 0.067 cm^2) and the cyt c_{552} diffusion coefficient ($D_o = 5 \times 10^{-6}$ cm^2 s^{-1}) determined from the simulation of the sweep rate dependent voltammetry (see below). This value of D_o is comparable with that reported for other *c*-type cytochromes [35]. The concentration of cyt c_{552} under the membrane estimated with this method is only upper bound and will be less than this depending on how much of the current is from the surface adsorbed protein.

3.3. Catalytic voltammetry

The mediated catalytic voltammetry of NT-26 Aio with its physiological electron acceptor cyt c_{552} on a Au/MUA electrode in 100 mM phosphate buffer (pH 6) is illustrated in Fig. 2. In the absence of arsenite (curve a), the redox response of cyt c_{552} is unaltered upon introduction of 1 μL of 26 μM NT-26 Aio under the membrane of the Au/MUA/cyt c_{552} electrode. This shows that the enzyme does not perturb interactions between cyt c_{552} and the electrode. The redox peak potential and its peak to peak separation are almost identical to that seen in Fig. 1 without Aio present.

Upon addition of 640 μM arsenite to the electrochemical cell (Fig. 2, curve b), the anodic current is amplified and the cathodic peak vanishes completely; characteristic of a catalytic homogeneous reaction coupled to heterogeneous electron transfer (EC′ mechanism) [31]. Here arsenite is oxidized and enzymatically yielding a reduced form of NT-26 Aio (Aio_{red}, Scheme 2), which is oxidized again by electrogenerated cyt c_{552}.

In separate experiments, we found no change in the redox wave of cyt c_{552} alone upon addition of 1 mM of arsenite to the electrochemical cell, which demonstrates that direct oxidation of arsenite by cyt c_{552} (or at the electrode) does not occur. Similarly no direct electrochemistry of Aio was observed in the absence of cyt c_{552} regardless of whether arsenite was present or not (Supporting information Fig. S3).

Fig. 3 presents the voltammetry in the presence of increasing concentrations of arsenite. At low arsenite concentrations (<100 μM) a pre-wave is observed at +200 mV in addition to the main redox wave of cyt c_{552} at +280 mV. The pre-wave grows steadily in magnitude with increasing substrate concentration and gradually replaces

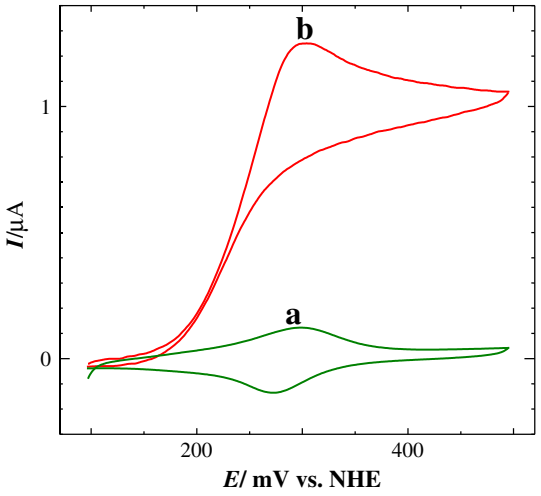

Fig. 2. CVs obtained for 1 μL of 26 μM NT-26 Aio and 4 μL of 64 μM cyt c_{552} on Au/MUA electrode in the absence (a, red) and presence (b, green) of 640 μM arsenite in 100 mM phosphate buffer solution (pH 6) at a scan rate of 5 mV s^{-1}.

the higher potential (uncoupled) cyt c_{552} wave which completely disappears at 400 μM arsenite (Fig. 3).

The pre-wave is associated with the coupled catalytic Aio–arsenite reaction but depletion of arsenite in the vicinity of the electrode results in the CV reverting to that of the uncoupled cyt c_{552} response at ca. +280 mV when the supply of substrate is exhausted [38]. A similar phenomenon was reported by our group recently with the mediated voltammetry of DMSO reductase on a glassy carbon electrode [39]. The catalytic peak potential shifts to higher potential with increasing arsenite concentration. Moreover, the initially asymmetric voltammograms at low arsenite concentration are transformed into a more symmetrical, sigmoidal wave form at approximately 1 mM of arsenite indicative of a steady state i.e. the oxidized form of cyt c_{552} is consumed by Aio at the same rate that it is regenerated at the electrode surface [40].

3.3.1. Aio–cyt c_{552} reaction

The reaction between cyt c_{552} and NT-26 Aio takes place in two consecutive one-electron outer sphere cross reactions (Scheme 2), while the ferric cytochrome (cyt c_{552ox}, Scheme 2) is regenerated by interfacial electron transfer at the Au/MUA surface. The waveform is very dependent on sweep rate. At slow sweep rates (Fig. 4, 2 mV s^{-1}) the concentration of cyt c_{552ox} at the electrode surface approaches a steady state as it is reduced by Aio_{red} at a similar rate as it is reoxidized by the electrode. As the sweep rate increases (Fig. 4, 20 and 50 mV s^{-1}) the concentration of cyt c_{552ox} formed at the electrode increases (linearly with sweep rate) and quickly exceeds that of the Aio. As there is now insufficient Aio_{red} (formed through arsenite oxidation) to reduce cyt c_{552ox}, the CV gradually returns to that of the uncoupled cyt c_{552ox}/c_{552red} system (cf. Fig. 2) masking the smaller catalytic sigmoidal wave.

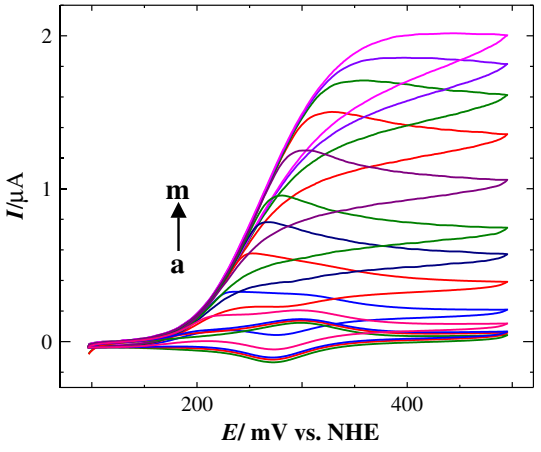

Fig. 3. CVs obtained for varying arsenite concentrations at Au/MUA/cyt c_{552}/NT-26 Aio electrode in 100 mM phosphate buffer at a sweep rate of 5 mV s^{-1} (a) 0, (b) 10, (c) 20, (d) 50, (e) 100, (f) 200, (g) 300, (h) 400, (i) 600, (j) 800, (k) 1000, (l) 1200 and (m) 1400 μM arsenite.

3.3.2. pH dependence

The electrocatalytic arsenite oxidation reaction at the Au/MUA/cyt c_{552}/Aio electrode was investigated within the range 4.5 < pH < 7.5 in a 100 mM citric acid–phosphate buffer mixture. Fig. 5 illustrates the maximum catalytic current as a function of pH. The catalytic current exhibits a pH optimum of 6.5 and it is consistent with the pH optimum (6.3) obtained from direct protein film voltammetry of NT-26 Aio [23]. However, it is somewhat higher than what was reported from solution assay using dichlorophenolindophenol (DCPIP) as electron acceptor (pH 5.5) [21].

The bell shaped catalytic profile was modeled with Eq. (2) for a system that is deactivated by either protonation (pK_{a1} = 5.1) or deprotonation (pK_{a2} = 7.5). Furthermore, the pH profile was independent of the direction of titration and catalytic activity was fully restored when the pH was returned to its optimal value. The pH window for catalytic activity is slightly broader than what was found for direct electrochemistry of NT-26 Aio on EPG electrode (pK_{a1} = 6.0 and pK_{a2} = 6.5) [23], but the differences are modest given the variations in working electrode (EPG vs. Au/MUA), the use of an electron transfer mediator here and the experimental uncertainties in the calculated pK_a values (±0.2). As mentioned above, the cyt c_{552} voltammetry is pH-independent in this range so the pH dependence of catalytic current is linked to Aio activity but pH variations may also perturb the Aio/cyt c_{552} interaction. Above pH 7.5 the cyt c_{552} signal (even in the absence of Aio) diminishes (see Fig. S1) so no higher pH values could be examined.

3.3.3. Temperature dependence

The catalytic activity of NT-26 Aio was also investigated across the temperature range from 5 to 25 °C. It is apparent that catalytic activity increases with temperature as shown in Fig. 6. In addition to the increase in catalytic current, the oxidation peak potential shifts to lower potential upon increasing the temperature; +440 mV at 5 °C (curve a) compared to +400 mV at 25 °C (curve e). These experiments illustrate that the enzyme activity (catalytic current) drops by about a factor of two on cooling from 25 °C to 5 °C which is not unexpected from basic reaction kinetics [41].

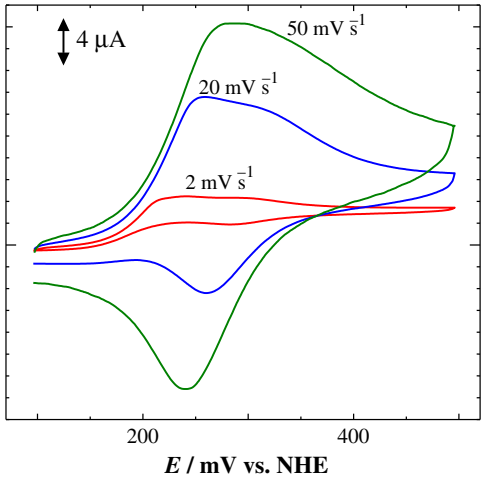

Fig. 4. CVs obtained for 100 μM arsenite at Au/MUA/cyt c_{552}/NT-26 Aio electrode in 100 mM phosphate buffer (pH 6) at sweep rates of 2, 20 and 50 mV s^{-1}.

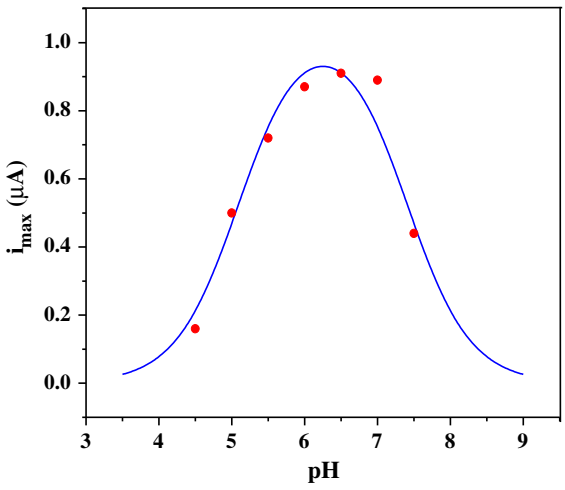

Fig. 5. pH dependence of the maximum oxidation current in the presence of 400 μM arsenite at the Au/MUA/cyt c_{552}/NT-26 Aio electrode at a scan rate of 5 mV s^{-1}. The solid curve is obtained from a fit to the experimental points using Eq. (2).

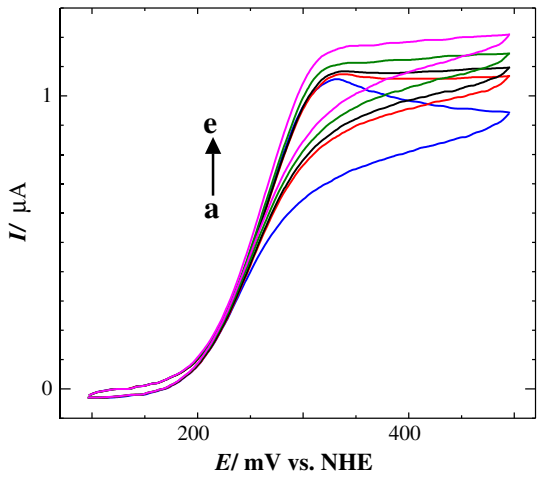

Fig. 7. Rotating disk voltammetry of Au/MUA/NT-26 Aio/cyt c_{552} with 600 μM arsenite (100 mM phosphate buffer solution, pH 6) at a scan rate of 5 mV s^{-1} at different rotation rates (a) 0, (b) 200, (c) 500, (d) 1000 and (e) 2000 rpm.

3.3.4. Mass transport limitations

Fig. 7 depicts the rotating disk voltammetry (RDV) of 600 μM of arsenite at the Au/MUA/NT-26 Aio/cyt c_{552} electrode at a scan rate of 5 mV s^{-1}. At a stationary electrode, the forward and backward scans are distinctly different i.e. the anodic scan shows tailing while the cathodic scan is sigmoidal (curve a). The observed transient wave is indicative of the depletion of arsenite within the diffusion layer during the forward (anodic) scan. At a rotation rate of 200 rpm, the forward and reverse scans begin to take on a similar shape as the depletion layer is narrowed and becomes time independent. As the rotation rate increases further (500 to 2000 rpm) the CVs begin to converge. This is because the Aio–arsenite reaction becomes rate (current)-limiting rather than mass transport of arsenite to the reaction layer. Above 2000 rpm, no significant changes in the voltammogram were observed either in shape or oxidation current.

3.3.5. Cation inhibition

We investigated the effect of various divalent metal ions on the electrocatalytic activity of the cyt c_{552}/NT-26 Aio system. No significant changes in the catalytic voltammetry were observed in the presence of 2 mM of Na^+, K^+, Ca^{2+}, Mg^{2+} and Mn^{2+} at a substrate concentration of 800 μM arsenite (data not shown). On the other hand, the catalytic current diminished to 5, 18, 35 and 38% of its initial value in the presence of 2 mM Zn^{2+}, Ni^{2+}, Co^{2+} and Fe^{2+} respectively. Fig. 8 represents an example for the effect of Zn(II) on cyt c_{552}/NT-26 Aio catalytic activity. Fig. 8 (curve a) shows the initial catalytic current (without Zn(II)) while Fig. 8 (curve b) shows that the catalytic signal is suppressed (<5% of original current) when Zn(II) is present. After rinsing the electrode and returning it to a fresh (Zn(II)-free) solution of arsenite the catalytic current was completely restored (Fig. 8, curve c).

Clearly the presence of Zn(II), Ni(II), Co(II) or Fe(II) ions has an inhibitory effect on the system but there are two important observations. No cyt c_{552} response was seen at all in the presence of Zn(II) ions (Fig. 8, curve b). If the enzyme Aio alone was inhibited by Zn(II) (or the other metal ions) then the catalytic voltammetry should revert to a simple reversible transient response from cyt c_{552} (as seen in Fig. 1). Instead the entire cyt c_{552} signal disappeared. Secondly the apparent inhibition was completely reversible by simply rinsing the electrode in fresh buffer then returning to a Zn(II)-free solution of arsenite (Fig. 8, curve c).

It is clear that Zn(II), Ni(II), Co(II) or Fe(II) interferes with electrochemically driven catalysis by disrupting the Au/MUA–cyt c_{552} interaction. Given that Fe(II), Co(II), Ni(II) and Zn(II) all have affinity

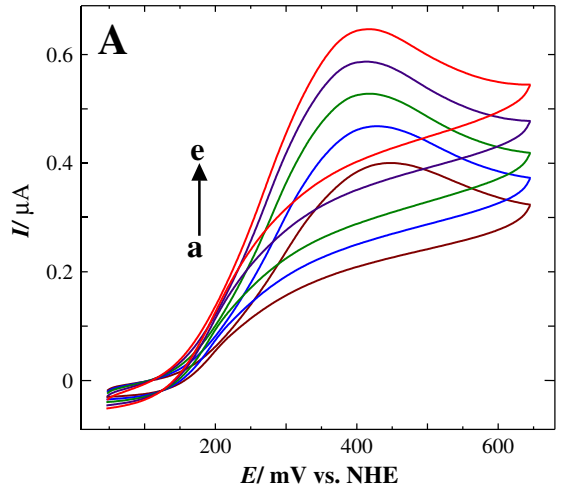

Fig. 6. CVs obtained for 200 μM arsenite at different temperatures (a) 5, (b) 10, (c) 15, (d) 20 and (e) 25 °C in 100 mM phosphate buffer (pH 6) at a scan rate of 5 mV s^{-1}.

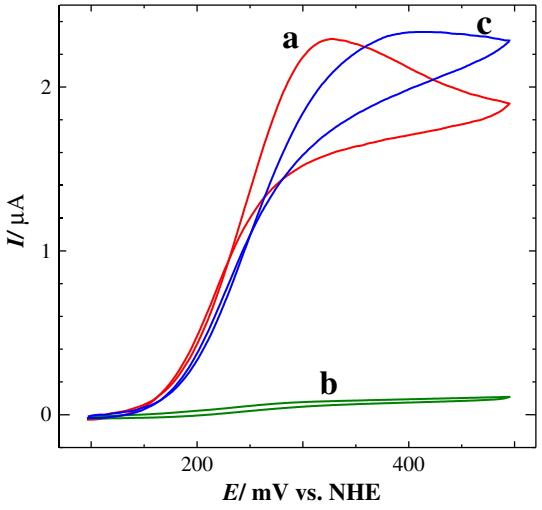

Fig. 8. CVs obtained for 800 μM arsenite at Au/MUA/cyt c_{552}/NT-26 Aio electrode in the absence (a) and presence (b) of 2 mM $ZnCl_2$ and (c) washed electrode in 800 μM arsenite (100 mM phosphate buffer solution (pH 6) and scan rate of 5 mV s^{-1}).

for carboxylato ligands (the terminal groups on the Au/MUA self-assembled monolayer) and the degree of inhibition roughly follows stability constant predictions from the Irving–Williams series (Zn(II) ~ Ni(II) > Co(II) > Fe(II)) [42], it emerges that the source of 'inhibition' in this case is the exchange of cyt c_{552} for electrochemically inert divalent cations on the Au/MUA surface. A similar phenomenon has been reported for horse heart cyt *c* on a Au/MUA electrode by Bowden and co-workers [43]. They found that the electrostatically adsorbed cyt *c* could be displaced from the Au/MUA electrode surface in the presence of high concentrations of competing cations [43]. We cannot gauge whether these divalent ions have any effect on Aio catalysis. If there is any genuine inhibitory effect by Zn(II), Ni(II), Co(II) or Fe(II) on Aio activity then it is reversible.

3.3.6. Anion inhibition

Many anions may potentially act as competitive inhibitors for the Mo active site. The most obvious is the product arsenate, which will be bound to the reduced Mo active site immediately following turnover. However, we observed no effect on catalysis up to arsenate concentrations of 2 mM (in the presence of 800 μM arsenite) so product inhibition can be ruled out. All electrochemical experiments were carried out in phosphate buffer (100 mM) but this anion may potentially interact with the active site particularly at such relatively high concentrations. Lowering the phosphate concentration from 100 mM to 20 mM had no influence at all on the catalytic current (Supporting information Fig. S4) so phosphate appears to have no significant inhibitory effect on Aio catalysis.

3.4. Electrochemical simulation

The rate constants defined in Scheme 2 collectively influence the observed CVs and in principle with all of these values known, it is possible to reproduce the experimental CV at different substrate concentrations and sweep rates using electrochemical simulation. In recent years, we have employed digital simulation of the mediated electrochemistry of molybdoenzymes such as DMSO reductase [44] and xanthine dehydrogenase [45] to provide new insight into the kinetics of the enzyme catalytic mechanisms which are not accessible from steady state or stopped flow kinetic studies.

Parameters such as diffusion coefficients, heterogeneous electron transfer rates and electrode surface area were measured in the absence of any homogeneous coupled reactions (see Experimental section).

3.4.1. Sweep rate dependence

The voltammetric sweep rate is a significant variable to elucidate the kinetics of electrochemical processes coupled with chemical reactions and the DigiSim program [34] enables the same set of parameters to be optimized to CVs measured at a variety of sweep rates. The comparison of experimental and simulated voltammetry at various sweep rates (2 to 20 mV s^{-1}) is given in Fig. 9 for two different arsenite concentrations. Representative scan rate dependent simulated voltammograms recorded at function of various substrate concentrations are given in the Supporting information (Fig. S5).

As can be seen from Fig. 9A, at a moderate concentration of arsenite (100 μM) and low sweep rate (2 mV s^{-1}) the highly unusual and distorted CVs are well reproduced comprising the catalytic pre-wave (at lower potential) convoluted with the conventional reversible response from cyt c_{552} uncoupled from the catalytic reaction as discussed above (and see Fig. 4). At these low arsenite concentrations the catalytic reaction is limited by substrate binding which enabled an accurate value of k_1 (1×10^6 M^{-1} s^{-1}) to be obtained; lower values led to a much worse fit. The arsenate dissociation rate (k_3) was not accurately determined as the simulated CV was insensitive to 2-fold lower and 20-fold higher values so this step appears to never be rate-limiting. This is consistent with the lack of arsenate inhibition found experimentally (see above).

3.4.2. Substrate concentration dependence

The same set of parameters was employed to simulate the arsenite concentration dependent catalytic CVs. Fig. 10 displays the response of Au/MUA/cyt c_{552}/NT-26 Aio electrode as function of arsenite concentration. Substrate depletion at low arsenite concentration is gradually overcome as the substrate concentration increases as mentioned earlier and these effects are reproduced by the simulation. In these cases, the simulation was most sensitive to the turnover number (k_2) and cross reaction rate constant between cyt c_{552} and NT-26 Aio (k_4).

3.4.3. Analysis of kinetic parameters

The rate and equilibrium constants defined in Scheme 2 and given in Table 1 reproduced all experimental CVs across a range of sweep rates and arsenite concentrations. The slope (or steepness) of the catalytic wave reflects the stoichiometry of the electron transfer event that initiates catalysis [46]. As cyt c_{552} is an obligate one electron acceptor the slope of the sigmoidal wave at its inflection point is consistent with this stoichiometry. The obtained parameters are summarized in

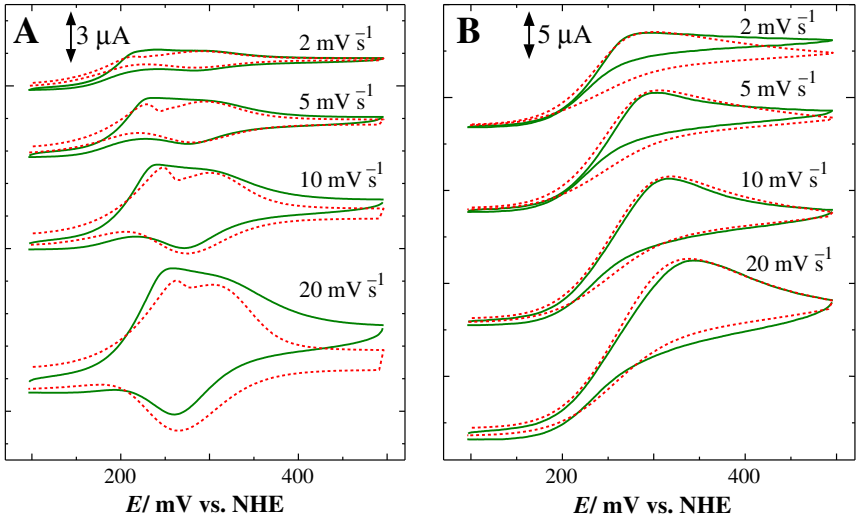

Fig. 9. Experimental (solid lines) and simulated (broken lines) sweep rate dependent CVs obtained for (A) 100 and (B) 600 μM arsenite at Au/MUA/cyt c_{552}/NT-26 Aio electrode in 100 mM phosphate buffer (pH 6).

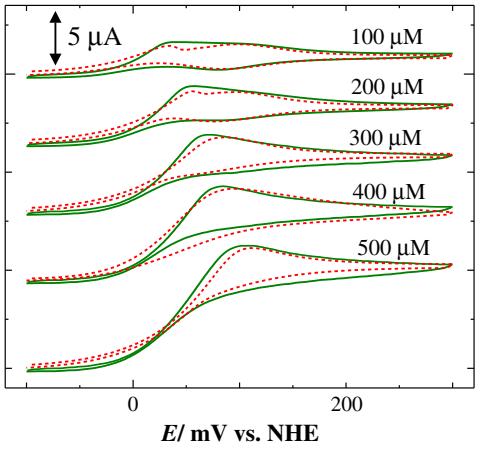

Fig. 10. Experimental (solid lines) and simulated (broken lines) CVs obtained for varying arsenite concentrations at the Au/MUA/cyt c_{552}/NT-26 Aio electrode in 100 mM phosphate buffer (pH 6) at a scan rate of 10 mV s^{-1}.

Table 1 and compared with some of the values reported by conventional solution assays with DCPIP as the electron acceptor [7].

The accurate simultaneous fitting of multiple variables in a simulation is problematic due to some parameters having no influence on the simulated CV in some cases. It was important to refine parameters under appropriate experimental conditions. For example, the substrate binding rate constant (k_1) was most accurately determined at low arsenite concentrations. The very large value of k_1 would be difficult to measure directly. Apart from its magnitude, the binding of arsenite to the Mo(VI) active site would be spectroscopically undetectable as no change in the coordination sphere of the active site occurs.

It is also noted that the apparent turnover number ($k_2 = 1\ s^{-1}$) is correlated with the Aio concentration under the membrane and this is quite variable depending on the internal volume so this parameter is not determined with accuracy. The value that has been obtained from solution assays with DCPIP as electron acceptor is $k_2 = 8.6\ s^{-1}$ [7] so this is a sensible upper bound. The apparent K_M [$K_{M,app} = (k_2 + k_{-1})/k_1$] obtained from the simulation parameters is 910 μM, which is significantly higher than that reported from solution assays (61 μM) with DCPIP as electron acceptor [7]. Apart from a lower than usual apparent turnover number (k_2) the actual determined substrate binding rate constant (k_1) may even be underestimated here due to arsenite diffusion being slowed by the membrane in which it must traverse when diffusing to the enzyme. The product release rate (k_3), dissociation of arsenate from reduced NT-26 Aio, was not rate-limiting under the conditions explored here, even in the presence of elevated concentrations of added arsenate. Therefore the obtained k_3/k_{-3} values are determined by low accuracy.

The rate constant k_4 was modeled as a simple outer sphere electron transfer reaction. In principle the reaction between Aio and cyt c_{552} should follow Michaelis–Menten kinetics (binding, electron transfer and dissociation) but this analysis is impractical electrochemically as it would require the cyt c_{552} concentration to be varied with a new electrode and membrane being prepared for each cyt c_{552} concentration dependent CV. The possible variations in SAM coverage on each electrode (from one experiment to the next) would present challenges in measuring comparable catalytic currents. An alternative would be to remove the membrane altogether and utilize bulk solution concentrations of Aio and cyt c_{552}. This would require very large amounts of each protein (~1 mg) per experiment in a cell volume of ~5 mL to achieve sufficiently high (micromolar) concentrations to see significant electrochemical activity. Solution kinetics of Aio with cyt c_{552} as electron acceptor will be reported separately.

Table 1
Parameters derived from electrochemical simulation. Values bracketed are from Ref. [7].

E^o (mV vs. NHE)	+275
k_1 ($M^{-1}\ s^{-1}$)	1.0×10^6
k_{-1} (s^{-1})	909
k_2 (s^{-1})	1 (8.6)
k_{-2} (s^{-1})	0.1
k_3 (s^{-1})	250
k_{-3} ($M^{-1}\ s^{-1}$)	0.6
k_4 ($M^{-1}\ s^{-1}$)	2.1×10^5
k_{-4} ($M^{-1}\ s^{-1}$)	104
$K_{M,app\ (arsenite)}$ (μM)	910 (61)

4. Conclusions

The mediated electrocatalytic voltammetry of NT-26 Aio with its native electron partner cyt c_{552} has been demonstrated for the first time and our quantitative investigation of the Aio/arsenite/cyt c_{552} system encompassing electrochemical simulation of the experimental data is the first of its kind for a Mo enzyme. In the absence of arsenite, or Aio, cyt c_{552} exhibits a well-defined single electron reversible response at a Au electrode modified with the long chain mercaptoundecanoic acid, which presents a self-assembled monolayer of negatively charged functional groups to the protein surface. In the presence of arsenite and Aio a variety of CV waveforms are observed depending on sweep rate and substrate concentration. Digital simulation revealed that arsenite binding is very fast (too fast to be measured directly by rapid mixing kinetics) and the outer sphere electron transfer cross reaction rate was also determined.

Acknowledgements

The Australian Research Council is acknowledged for their financial support (DP120101465). MDH was funded by a Medical Research Council PhD studentship (G0800112) and his work in Australia was funded by the Society for General Microbiology Presidents' fund.

Appendix A. Supplementary data

Supplementary data to this article can be found online at http://dx.doi.org/10.1016/j.bbabio.2013.07.010.

References

[1] R.S. Oremland, J.F. Stolz, The ecology of arsenic, Science 300 (2003) 939–944.
[2] R. Eisler, Arsenic hazards to humans, plants, and animals from gold mining, Rev. Environ. Contam. Toxicol. 180 (2004) 133–165.
[3] B.P. Rosen, Biochemistry of arsenic detoxification, FEBS Lett. 529 (2002) 86–92.
[4] P.B. Tchounwou, A.K. Patlolla, J.A. Centeno, Carcinogenic and systemic health effects associated with arsenic exposure—a critical review, Toxicol. Pathol. 31 (2003) 575–588.
[5] M.-C. Lett, D. Muller, D. Lièvremont, S. Silver, J. Santini, Unified nomenclature for genes involved in prokaryotic aerobic arsenite oxidation, J. Bacteriol. 194 (2012) 207–208.
[6] H.H. Green, Description of a bacterium which oxidizes arsenite to arsenate, and of one which reduces arsenate to arsenite, isolated from a cattle-dipping tank, S. Afr. J. Sci. 14 (1918) 465–467.
[7] J.M. Santini, R.N. vanden Hoven, Molybdenum-containing arsenite oxidase of the chemolithoautotrophic arsenite oxidizer NT-26, J. Bacteriol. 186 (2004) 1614–1619.
[8] R.N. vanden Hoven, J.M. Santini, Arsenite oxidation by the heterotroph *Hydrogenophaga* sp. str. NT-14: the arsenite oxidase and its physiological electron acceptor, Biochim. Biophys. Acta Bioenerg. 1656 (2004) 148–155.
[9] G.L. Anderson, J. Williams, R. Hille, The purification and characterization of arsenite oxidase from *Alcaligenes faecalis*, a molybdenum-containing hydroxylase, J. Biol. Chem. 267 (1992) 23674–23682.
[10] K.S. Prasad, V. Subramanian, J. Paul, Purification and characterization of arsenite oxidase from *Arthrobacter* sp, Biometals 22 (2009) 711–721.
[11] A. Lieutaud, L.R. van, S. Duval, L. Capowiez, D. Muller, R. Lebrun, S. Lignon, M.-L. Fardeau, M.-C. Lett, W. Nitschke, B. Schoepp-Cothenet, Arsenite oxidase from *Ralstonia* sp. 22: characterization of the enzyme and its interaction with soluble cytochromes, J. Biol. Chem. 285 (2010) 20433–20441.
[12] T.H. Osborne, M.D. Heath, A.C.R. Martin, J.A. Pankowski, K.A. Hudson-Edwards, J.M. Santini, Cold-adapted arsenite oxidase from a psychrotolerant *Polaromonas* species, Metallomics 5 (2013) 318–324.

[13] T. Conrads, C. Hemann, G.N. George, I.J. Pickering, R.C. Prince, R. Hille, The active site of arsenite oxidase from *Alcaligenes faecalis*, J. Am. Chem. Soc. 124 (2002) 11276–11277.
[14] L. McNellis, G.L. Anderson, Redox-state dependent chemical inactivation of arsenite oxidase, J. Inorg. Biochem. 69 (1998) 253–257.
[15] E. Lebrun, M. Brugna, F. Baymann, D. Muller, D. Lievremont, M.-C. Lett, W. Nitschke, Arsenite oxidase, an ancient bioenergetic enzyme, Mol. Biol. Evol. 20 (2003) 686–693.
[16] C. Kisker, H. Schindelin, D. Baas, J. Retey, R.U. Meckenstock, P.M.H. Kroneck, A structural comparison of molybdenum cofactor-containing enzymes, FEMS Microbiol. Rev. 22 (1998) 503–521.
[17] R. Hille, The mononuclear molybdenum enzymes, Chem. Rev. 96 (1996) 2757–2816.
[18] P.J. Ellis, T. Conrads, R. Hille, P. Kuhn, Crystal structure of the 100 kDa arsenite oxidase from *Alcaligenes faecalis* in two crystal forms at 1.64 Å and 2.03 Å, Structure 9 (2001) 125–132.
[19] H. Sugimoto, S. Tatemoto, K. Suyama, H. Miyake, S. Itoh, C. Dong, J. Yang, M.L. Kirk, Dioxomolybdenum(VI) complexes with Ene-1,2-dithiolate ligands: synthesis, spectroscopy, and oxygen atom transfer reactivity, Inorg. Chem. 48 (2009) 10581–10590.
[20] R. van Lis, W. Nitschke, T.P. Warelow, L. Capowiez, J.M. Santini, B. Schoepp-Cothenet, Heterologously expressed arsenite oxidase: a system to study biogenesis and structure/function relationships of the enzyme family, Biochim. Biophys. Acta. 1817 (2012) 1701–1708.
[21] J.M. Santini, L.I. Sly, R.D. Schnagl, J.M. Macy, A new chemolithoautotrophic arsenite-oxidizing bacterium isolated from a gold mine: phylogenetic, physiological, and preliminary biochemical studies, Appl. Environ. Microbiol. 66 (2000) 92–97.
[22] S. Duval, J.M. Santini, W. Nitschke, R. Hille, B. Schoepp-Cothenet, The small subunit AroB of arsenite oxidase: lessons on the [2Fe–2S] Rieske protein superfamily, J. Biol. Chem. 285 (2010) 20442–20451.
[23] P.V. Bernhardt, J.M. Santini, Protein film voltammetry of arsenite oxidase from the chemolithoautotrophic arsenite-oxidizing bacterium NT-26, Biochemistry 45 (2006) 2804–2809.
[24] J.M. Santini, U. Kappler, S.A. Ward, M.J. Honeychurch, R.N. vanden Hoven, P.V. Bernhardt, The NT-26 cytochrome c552 and its role in arsenite oxidation, Biochim. Biophys. Acta Bioenerg. 1767 (2007) 189–196.
[25] K.B. Holt, Using scanning electrochemical microscopy (SECM) to measure the electron-transfer kinetics of cytochrome c immobilized on a COOH-terminated alkanethiol monolayer on a gold electrode, Langmuir 22 (2006) 4298–4304.
[26] M.C. Leopold, E.F. Bowden, Influence of gold substrate topography on the voltammetry of cytochrome c adsorbed on carboxylic acid terminated self-assembled monolayers, Langmuir 18 (2002) 2239–2245.
[27] T.P. Warelow, M. Oke, B. Schoepp-Cothenet, J.U. Dahl, N. Bruselat, G.N. Sivalingam, S. Leimkühler, K. Thalassinos, U. Kappler, J.H. Naismith, J.M. Santini, The respiratory arsenite oxidase: structure and the role of residues surrounding the Rieske cluster, PLoS One (2013), (Accepted for publication).
[28] R.M.C. Dawson, D.C. Elliot, W.H. Elliot, K.M. Jones, Data for Biochemical Research, 3rd ed. Science Publ., Oxford, 1986.
[29] J. Tkac, J.J. Davis, An optimized electrode pre-treatment for SAM formation on polycrystalline gold, J. Electroanal. Chem. 621 (2008) 117–120.
[30] K. Nakano, T. Yoshitake, Y. Yamashita, E.F. Bowden, Cytochrome c self-assembly on alkanethiol monolayer electrodes as characterized by AFM, IR, QCM, and direct electrochemistry, Langmuir 23 (2007) 6270–6275.
[31] A.J. Bard, L.R. Faulkner, Electrochemical Methods: Fundamentals and Applications, 2001.
[32] N. Anicet, C. Bourdillon, J. Moiroux, J.-M. Saveant, Electron transfer in organized assemblies of biomolecules. Step-by-step avidin/biotin construction and dynamic characteristics of a spatially ordered multilayer enzyme electrode, J. Phys. Chem. B 102 (1998) 9844–9849.
[33] M.S. Brody, R. Hille, The kinetic behavior of chicken liver sulfite oxidase, Biochemistry 38 (1999) 6668–6677.
[34] M. Rudolf, S.W. Feldberg, DigiSim Version 3.03b, Bioanalytical System, West Lafayette, 2004.
[35] M. Correia dos Santos, P.M.P. Sousa, G.M.L. Simoes, H. Lopes, I. Moura, J.J.G. Moura, Electrochemical studies on c-type cytochromes at microelectrodes, J. Electroanal. Chem. 464 (1999) 76–84.
[36] R.A. Clark, E.F. Bowden, Voltammetric peak broadening for cytochrome c/alkanethiolate monolayer structures: dispersion of formal potentials, Langmuir 13 (1997) 559–565.
[37] M.J. Eddowes, H.A.O. Hill, Electrochemistry of horse heart cytochrome c, J. Am. Chem. Soc. 101 (1979) 4461–4464.
[38] K. Yokoyama, Y. Kayanuma, Cyclic voltammetric simulation for electrochemically mediated enzyme reaction and determination of enzyme kinetic constants, Anal. Chem. 70 (1998) 3368–3376.
[39] K.-I. Chen, A.G. McEwan, P.V. Bernhardt, Mediated electrochemistry of dimethyl sulfoxide reductase from *Rhodobacter capsulatus*, J. Biol. Inorg. Chem. 14 (2009) 409–419.
[40] P.V. Bernhardt, Enzyme electrochemistry — biocatalysis on an electrode, Aust. J. Chem. 59 (2006) 233–256.
[41] A. Fersht, Enzyme Structure and Mechanism, W. H. Freeman and Co., San Francisco, 1977.
[42] H. Irving, R.J.P. Williams, Order of stability of metal complexes, Nature 162 (1948) 746–747.
[43] M. Collinson, E.F. Bowden, M.J. Tarlov, Voltammetry of covalently immobilized cytochrome c on self-assembled monolayer electrodes, Langmuir 8 (1992) 1247–1250.
[44] K.-I. Chen, A.G. McEwan, P.V. Bernhardt, Cobalt hexaamine mediated electrocatalytic voltammetry of dimethyl sulfoxide reductase: driving force effects on catalysis, J. Biol. Inorg. Chem. 16 (2011) 227–234.
[45] P. Kalimuthu, S. Leimkühler, P.V. Bernhardt, Catalytic electrochemistry of xanthine dehydrogenase, J. Phys. Chem. B 116 (2012) 11600–11607.
[46] H.A. Heering, J. Hirst, F.A. Armstrong, Interpreting the catalytic voltammetry of electroactive enzymes adsorbed on electrodes, J. Phys. Chem. B 102 (1998) 6889–6902.